Imaging Nutrient Distributions in Plant Tissue Using Time-of-Flight Secondary Ion Mass Spectrometry and Scanning Electron Microscopy[OA]

Ralf Metzner, Heike Ursula Schneider, Uwe Breuer, and Walter Heinz Schroeder*

Central Division of Analytical Chemistry (R.M., U.B.) and Phytosphere Institute (H.U.S., W.H.S.), Research Center Jülich, 52425 Julich, Germany

A new approach to trace the transport routes of macronutrients in plants at the level of cells and tissues and to measure their elemental distributions was developed for investigating the dynamics and structure-function relationships of transport processes. Stem samples from *Phaseolus vulgaris* were used as a test system. Shock freezing and cryo-preparation were combined in a cryogenic chain with cryo-time-of-flight secondary ion mass spectrometry (cryo-ToF-SIMS) for element and isotope-specific imaging. Cryo-scanning electron microscopy (cryo-SEM) was integrated into the cryogenic workflow to assess the quality of structural preservation. We evaluated the capability of these techniques to monitor transport pathways and processes in xylem and associated tissues using supplementary sodium (Na) and tracers for potassium (K), rubidium (Rb), and ^{41}K added to the transpiration stream. Cryo-ToF-SIMS imaging produced detailed mappings of water, K, calcium, magnesium, the K tracers, and Na without quantification. Lateral resolutions ranged from 10 μm in survey mappings and at high mass resolution to approximately 1 μm in high lateral resolution imaging in reduced areas and at lower mass resolution. The tracers Rb and ^{41}K, as well as Na, were imaged with high sensitivity in xylem vessels and surrounding tissues. The isotope signature of the stable isotope tracer was utilized for relative quantification of the ^{41}K tracer as a fraction of total K at the single pixel level. Cryo-SEM confirmed that tissue structures had been preserved with subcellular detail throughout all procedures. Overlays of cryo-ToF-SIMS images onto the corresponding SEM images allowed detailed correlation of nutrient images with subcellular structures.

Monitoring nutrient distributions in higher plant tissues is an important task for plant physiology. A selection of potent methods is available by analysis of single-cell samples, giving information on nutrient ion content of cell vacuoles (Rygol et al., 1993; Fricke et al., 1996; Tomos and Leigh, 1999). Fluorescent-dye ratio imaging can monitor free ions at the cell and tissue levels, giving symplastic or apoplastic concentrations (Mühling and Läuchli, 2000; Halperin and Lynch, 2003). However, as for measurements with ion-selective microelectrodes (Leigh, 2001), only a limited range of ions can be imaged, most commonly Ca^{2+} or K^+ ions in solution, but the total element contents, including bound species, are not detected.

At the tissue level, distributions of nutrients can be best revealed by microbeam analysis techniques, but they have been severely limited because satisfactory sample preparation methods have not yet been developed or detection sensitivities were not adequate. Our aim is to meet this challenge. It is essential that sample preparation preserves the original distribution of diffusible analytes. Chemical fixation or embedding leads to exchange or loss of material and must be avoided. By contrast, shock freezing can preserve the authentic distribution of solutes with minimal risk of redistribution because a sufficiently rapid solidification of water stops diffusion (Goldstein et al., 1992). Hypothetically, the shock-frozen, hydrated tissues may be simply freeze dried and then sectioned. However, besides possible relocation of solutes, freeze drying causes pronounced topography of the sectioned surfaces that will interfere dramatically with microbeam analysis. Therefore, the use of shock-frozen hydrated samples followed by the preparation of sample surfaces by fracturing and planing to eliminate surface topography is the method of choice for microbeam techniques that are currently available. If, and only if, samples are maintained below −80°C throughout all analytical procedures, this offers the best method to preserve in vivo ion distributions. A major limitation of this approach for samples much larger than a few cell layers (where vitrification is possible) is the formation of ice crystals during shock freezing. For samples with diameters as large as 2 mm that are needed for transport studies in complex tissues, ice crystal formation can only be minimized, but not avoided, and the structural preservation must be examined. Ice crystal formation is also responsible for the difficulties in obtaining cryo-sections under these conditions. The low temperatures are necessary to avoid recrystallization of water that may lead to redistribution of ana-

* Corresponding author; e-mail w.schroeder@fz-juelich.de.

The author responsible for distribution of materials integral to the findings presented in this article in accordance with the policy described in the Instructions for Authors (www.plantphysiol.org) is: Walter Heinz Schröder (w.schroeder@fz-juelich.de).

[OA] Open Access articles can be viewed online without a subscription.

www.plantphysiol.org/cgi/doi/10.1104/pp.107.109215

lytes and severe tissue damage. Most previous microbeam analyses on frozen-hydrated plant specimens have been obtained by energy-dispersive x-ray analysis (EDXA). With this technique, distributions of several nutrient elements at the cellular level were obtained (Canny, 1993; Williams et al., 1993). However, the detection sensitivity of cryo-EDXA for physiologically relevant elements is rather limited (approximately 10–20 mM for the usual macro- and micronutrients; Enns et al., 1998; Rowan et al., 2000) and often restricted to elements that are of high natural abundance or hyperaccumulated as, for example, in the analysis of zinc in leaves of *Thlaspi caerulescens* (Küpper et al., 1999).

Time-of-flight secondary ion mass spectrometry (ToF-SIMS) offers exceptional sensitivity that can, in principle, detect all elements and isotopes. ToF-SIMS is a surface analytical technique that is well established in material sciences (Vickerman, 2001). A pulsed scanning primary ion beam is used to sputter secondary ions from the surface of a solid sample. These secondary ions are transferred to a mass spectrometer to produce mass-resolved maps of element distributions. The immediate atomic vicinity of the analyte (the matrix) influences the efficiency to produce secondary ions. Cryo-ToF-SIMS on frozen-hydrated samples has rarely been employed, especially in plant physiology. So far, attempts to implement an uninterrupted cryo-chain were successful only in a few cases of biological suspensions (Colliver et al., 1997; Cliff et al., 2003) and only in three cases for the analysis of plant tissues (Dérue et al., 1999, 2006a; Dickinson et al., 2006). First successful cryo-SIMS studies on frozen-hydrated plant tissues used stems of flax (*Linum usitatissimum*) to localize sodium (Na), magnesium (Mg), calcium (Ca), and potassium (K; Dérue et al., 2006a) and leaf blades of *Pteris vittata* to map arsenic (Dickinson et al., 2006).

Allocation and transport of nutrients are typically dynamic processes related to changes in source-sink relationships and depend, for example, on growth and environmental conditions. Transport can be studied by use of tracers provided their transport properties reflect the nutrient of interest. Many investigations with techniques other than cryo-SIMS used a variety of element tracers based on the assumption that their chemical properties are similar to the element of interest (e.g. rubidium [Rb] for K or strontium [Sr] for Ca; Storey and Leigh, 2004). The interpretation of the resulting distribution patterns, however, can be problematic if a tracer does not mimic the respective nutrient completely (Marschner and Schimansky, 1968; Jeschke, 1970). Also, the similarities may depend on the context. For example, the similarity of Rb to K may be sufficient to trace apoplastic transport of K; on the other hand, it is known that transport of Rb and K across membranes depends on the selectivity of the K channels (Hedrich and Schroeder, 1989; Reintanz et al., 2002). Chemically identical isotopes are always preferable because of their identical transport characteristics (Schroeder et al., 1980; Schroeder and Fain, 1984). Isotope tracers and Rb have been used in the past for transport studies involving MS, including SIMS (Lazof et al., 1992; Goldsmith et al., 1993).

In this feasibility study, we implemented a completely cryogenic workflow to measure the distribution of nutrients in stem cross sections of French bean (*Phaseolus vulgaris* 'Shiny Fardenlosa') plants. The workflow is a sequence of shock freezing, cryo-preparation, cryo-ToF-SIMS, and cryo-scanning electron microscopy (cryo-SEM). Two tracers for K, Rb and enriched ^{41}K, were added to the transpiration stream to test the utility of the technique to measure their transport in xylem vessels and into surrounding tissues.

RESULTS AND DISCUSSION

Cryo-SEM Imaging as Control of Sample Preparation and Support for Cryo-ToF-SIMS Analysis of Frozen-Hydrated Stem Samples of French Bean

An important prerequisite for microbeam analysis is adequate tissue sample preparation. We therefore imaged the shock-frozen samples both before and after cryo-ToF-SIMS analysis. Because cryo-ToF-SIMS is a surface analytical technique, we planed cross-sectional fracture faces and evaluated their quality for element mapping by cryo-SEM. The fracture faces represent stem cross sections. Following the cryo-ToF-SIMS analysis, the sample surfaces were imaged again by cryo-SEM to evaluate for possible beam damage. Further, after cryo-ToF-SIMS analysis, it was possible to remove a thin layer of ice from the sample surfaces by freeze etching and examine the structural details that were invisible in the fully hydrated state. In this way, the structural preservation of tissues and cells could be verified.

Quality Control of Sample Surfaces Prepared for Cryo-ToF-SIMS

Fracture faces of frozen-hydrated samples were imaged by cryo-SEM prior to cryo-ToF-SIMS analysis. A typical image of a French bean stem segment is shown in Figure 1. The micrograph represents about 15% of the total surface area of the sample. As judged by cryo-SEM imaging, large surface areas of the samples appeared sufficiently flat for cryo-ToF-SIMS analysis. Almost no structural details of the tissue under investigation can be recognized, except for a few semicircular white lines delineating the lumina of some xylem vessels (the largest marked with X in Fig. 1) by local sample charging due to the conductivity of the underlying structures and not by topography. Minor knife marks running from bottom left to top right are visible (marked by arrows in Fig. 1), indicating that no water sublimation from the surface had occurred during sample preparation. Minor knife marks were not detectable in cryo-ToF-SIMS images; however, larger marks could result in topography

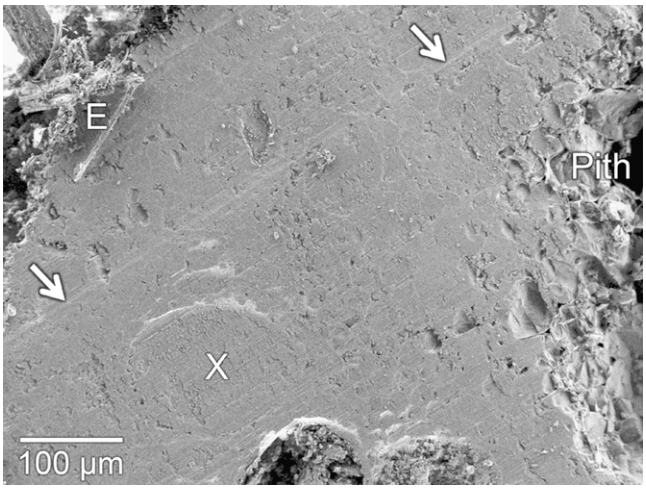

Figure 1. Cryo-SEM micrograph of a cross-sectional face of a shock-frozen, hydrated stem segment of French bean. The surface was planed for cryo-ToF-SIMS analysis and imaged by cryo-SEM to ascertain that large enough areas of little topography were available for analysis. Some minor knife marks are visible (arrows). E, Epidermis; Pith, pith cells; X, xylem vessel.

effects. The lack of water loss is also confirmed by a lack of prominent cell structures above the ice plane. Confined areas of pronounced topography could be occasionally detected, such as in the part of the sample surface labeled as pith in Figure 1, where cells are missing or damaged. Figure 1 also shows two xylem vessels lacking water (bottom middle) and protruding uncut fibers (top left corner) near the epidermis. Once the planing procedure was optimized, pronounced surface irregularities could be recognized by light microscopy (data not shown). Consequently, surface quality control prior to cryo-ToF-SIMS analysis was reduced to light microscopic monitoring of the sample surface during the planing process and in the cryo-ToF-SIMS instrument.

Cryo-SEM Imaging after Cryo-ToF-SIMS Analysis

Sample surfaces were routinely imaged by cryo-SEM after completion of the cryo-ToF-SIMS analysis, maintaining an uninterrupted cryo-chain. Scanned areas were undistinguishable from surrounding unscanned areas, indicating that no beam damage had occurred during cryo-ToF-SIMS analysis that was detectable by the field emission cryo-SEM (data not shown).

For quality control of tissue preservation, the cellular and tissue structures buried in the ice had to be revealed by freeze etching of the sample surfaces. To this end, the temperature of the sample holder was transiently elevated to approximately −90°C. Water sublimation from the specimen surface was monitored by continuous imaging. The image shown in Figure 2A is typical of a total number of 30 shock-frozen samples of French bean stems analyzed by cryo-ToF-SIMS and cryo-SEM. One assembly of proto- and metaxylem vessels and several secondary xylem vessels, as well as the phloem, cambium, and pith, are distinguishable due to cell shapes and sizes and cell wall thickness. Despite the large size of the stem samples with diameters of 2 to 2.5 mm that will lead to at least some structural damage due to ice crystal formation during shock freezing, subcellular structures (vacuoles and organelles) were preserved in many tissue areas (Fig. 2B). The structural preservation within the block faces therefore appears sufficient for tissue level and, to some extent, even subcellular cryo-ToF-SIMS analysis. Ice crystal formation had obviously occurred in most vessels and cells during shock freezing. Ice crystals can be detected by the striped appearance in the lumina (Fig. 2A). Such structures are typical for sample areas of high water content. Solutes interfere with the crystalline structure of pure water and therefore are often squeezed out during crystal growth. This results in the accumulation of solutes between the ice crystals in so-called interdendritic channels. Whereas the water is removed from the sample surface by sublimation, the solutes remain and become apparent in ordered structures.

No indication of ice crystal growth traversing cell walls was found. Structural damage at the tissue level was absent in most areas of the samples, but local tissue defects, as indicated by arrows in Figure 2A, were occasionally visible. Areas of such imperfections were in retrospect excluded from interpretation of the cryo-ToF-SIMS data.

An interesting finding of cryo-SEM during freeze etching the samples was that sublimation was not homogeneous, but different rates of sublimation could be observed during the process of freeze etching. This resulted in a variety of final ice levels in different tissues as visible in Figure 2 and may be caused by local differences in solute or free water concentrations and/or water-binding capacities that might be specific for cells or tissues. Some cells in the phloem region still contained frozen cell sap up to the plane of cutting, whereas the xylem vessels exhibited ice levels well below this plane. Even lumina belonging to the same tissue type could exhibit different sublimation properties. This applies to xylem vessels as well as to phloem cells. Note, for example, the slightly different ice level of xylem vessel X1 as opposed to those of vessels X2 and X3 and the very deep etching of the very small vessels adjacent to X2 and X3. Qualitative evaluation of seven similar cryo-SEM images indicated that there may be a general tendency to stronger etching of smaller vessels (data not shown). However, there may be a more complex situation and further study is needed before conclusions can be drawn.

Evaluation of Cryo-ToF-SIMS Imaging of Naturally Occurring Elements and Tracers

To test the suitability of our analytical protocols to study the distribution and the transport of nutrient

Figure 2. Cryo-SEM micrographs of cross-sectional faces of frozen-hydrated internodal stem segments of French bean obtained after cryo-ToF-SIMS analysis. Freeze etching was applied to reveal details of tissues and cell structures for quality control of the structural preservation, as well as reference to cryo-ToF-SIMS ion images. A, Overview of the tissue types in the vascular tissues, from an area that was already analyzed by cryo-ToF-SIMS. Starting from the lower left corner of the image, the phloem (Ph) can be seen, separated by the cambium (Cam) from the xylem. The xylem is in the secondary state of growth as indicated by the presence of large secondary vessels (X1–X3) as well as smaller vessels, and metaxylem vessels are bordering X2 (probably metaxylem) on the top right side and small secondary vessels bordering X3 on the top. All vessels are enclosed by xylem parenchyma (XP). Toward the pith (Pith) thicker cell walls are visible, while toward the cambium, the xylem parenchyma is more thin walled. Occasional local tissue defects are visible (arrows). B, Detailed view of xylem and surrounding tissues, including subcellular structural details, such as the fine structure of xylem walls, vacuoles, and organelles in xylem parenchyma cells. The arrows are placed in vacuoles and point to organelles in the cytoplasm.

elements, we examined whether (1) the most abundant isotopes of some common cationic nutrient elements could be localized in the frozen-hydrated sample surfaces with a satisfactory quality; and (2) Rb and ^{41}K distribution from xylem vessels into the surrounding tissues could be traced satisfactorily.

In this pilot study, we used freshly detached shoots of French bean plants that were fed from their cut end with tracer solutions. Tracers added to the transpiration stream were either applied in half-strength Hoagland solution (solution 1) containing 10 mM Rb or in a stable isotope solution (solution 2) containing

2.5 mM enriched ^{41}K. The tracer concentrations were near physiological concentrations found in other plant species (Lohaus et al., 2000; Herdel et al., 2001; Wegner and Zimmermann, 2002). After a 20-min application of the solution to the transpiration stream, stem samples were harvested approximately 50 cm apical of the application site for subsequent processing for cryo-ToF-SIMS.

Cryo-ToF-SIMS Imaging of Naturally Occurring Elements at 10-μm Lateral Resolution

The first cryo-ToF-SIMS images shown are recorded in the high-current bunched mode, which has two advantages. First, it allows imaging of large tissue areas up to 500 $\times$ 500 μm^2 within a reasonable measurement time, typically 3 to 4 h. Second, it offers a high mass resolution of $m/\Delta m$ = 3,500. This allows the necessary unambiguous identification of the ion species of interest and separation from potentially interfering ions (e.g. hydrocarbons and water clusters). The lateral resolution of 10 μm permits the recognition of individual tissues based on differences in cell shape that was verified by cryo-SEM images obtained from the same sample.

An example of a set of cryo-ToF-SIMS images is shown in Figure 3. These images were obtained from the same area that was subsequently imaged after freeze etching by cryo-SEM (Fig. 2A). The analyzed sample was obtained after feeding with a Rb tracer (solution 1).

Contrast in such SIMS images is derived from (1) the local variation in concentration of the analyte; (2) the topography of the specimen surface (Rangarajan and Tyler, 2006); and (3) the local matrix composition (Vickerman, 2001). The surface topography in our sample preparation was sufficiently reduced to avoid interference with the imaging process because minor knife marks that were detectable by cryo-SEM never appeared in ion images. Matrices of biological tissues are highly complex and inhomogeneous and this may modulate the local ion signal leading to artefacts. Despite this general caveat, it is plausible that within the hydrated tissue the matrix is similar throughout the imaged area. Another caveat is that different signals between elements (Wilson et al., 1989) in an unknown matrix do not allow relative quantification of the elements. In the well-studied case of pure silicon, the yields of elements of the first main group in the periodic table are by a factor of 3 to 5 higher than those of the second main group (Wilson et al., 1989; due to the higher ionization energy of the second group). Dérue et al. (2006b) determined sensitivity factors for Na, Mg, and Ca relative to K using frozen-hydrated reference solutions and found factors for Na/K as 0.67; Mg/K as 0.22; Ca/K as 0.31. These sensitivity factors were obtained under different SIMS conditions and may not be applicable to our conditions. Nevertheless the prospects for quantification are promising for cryo-ToF-SIMS due to the lower erosion depth as compared to dynamic SIMS.

The distribution of water in this sample is represented in Figure 3A by $^{1}H_{3}{}^{16}O^{+}$, the most abundant water-related ion species. The image confirms the hydrated state of the sample because $^{1}H_{3}{}^{16}O^{+}$ ions were detected in almost the entire imaged area. Several xylem vessels, including the large vessels termed X1 to X3 in Figure 2A and a number of larger and smaller cells, are prominent in Figure 3A due to contrast between higher signals in lumina compared to cell borders. Pronounced differences in ion signals between different tissue areas of the sample are visible. The highest signals are found in xylem vessels X2 and X3 and adjacent smaller vessels, as well as in pith cell lumina. Xylem parenchyma, cambium, phloem, and xylem vessel X1 exhibit lower signals. This is compatible with the speculations about the different tissue components derived from the differences in ice levels observed by cryo-SEM after freeze drying (Fig. 2).

In addition to water, we show the major naturally occurring isotopes of K ($^{39}K^{+}$; Fig. 3B), Mg ($^{24}Mg^{+}$; Fig. 3C), and Ca ($^{40}Ca^{+}$; Fig. 3, D and E). K (Fig. 3B) could be imaged with particularly high sensitivity because of its high ionization probability. Together with the high abundance of this major cation in living plant tissues, this resulted in K images of especially high signals. The highest $^{39}K^{+}$ signals originate from the thick-walled xylem parenchyma and some hot spots in the pith. Some cells abutting xylem vessel X2 also reveal particularly high signals. Lower signals are found in most areas of the pith, the thin-walled xylem parenchyma, the cambium, and the phloem. The contents of xylem vessels X2 and X3 appear as dominating dark structures. Compared to these xylem vessels, the lumen of vessel X1 exhibits 4-fold higher $^{39}K^{+}$ signals (440–1,750 mean counts/pixel). Likewise, Enns et al. (1998) found higher concentrations of K in certain xylem vessel elements compared to the bulk of vessels analyzed in a study on frozen-hydrated maize (*Zea mays*) roots with EDXA. They suggested that these high K concentrations indicate that these vessel elements were not fully mature, which we assume applies as well for vessel X1.

The particularly differentiated distribution of $^{24}Mg^{+}$ (Fig. 3C) shows a high signal in a distinct band of the thin-walled xylem parenchyma cells close to the vessels and the cambium. Also, cells abutting xylem vessels X1 and X2 and facing toward the cambium and phloem exhibit markedly higher signals compared to the neighboring tissues. Lowest $^{24}Mg^{+}$ signals are found in the xylem vessels, phloem, pith, and cambium. The confined distribution pattern may indicate a specialization of these cells for Mg uptake and accumulation. A similar assumption was made by Shaul et al. (1999) on the basis of a study on Arabidopsis (*Arabidopsis thaliana*), which showed an enrichment of mRNA for the Mg^{2+}/H^{+} exchanger AtMHX in close association with the vascular elements. They hypothesized that this exchanger may be responsible for creating a vacuolar pool of Mg^{2+}

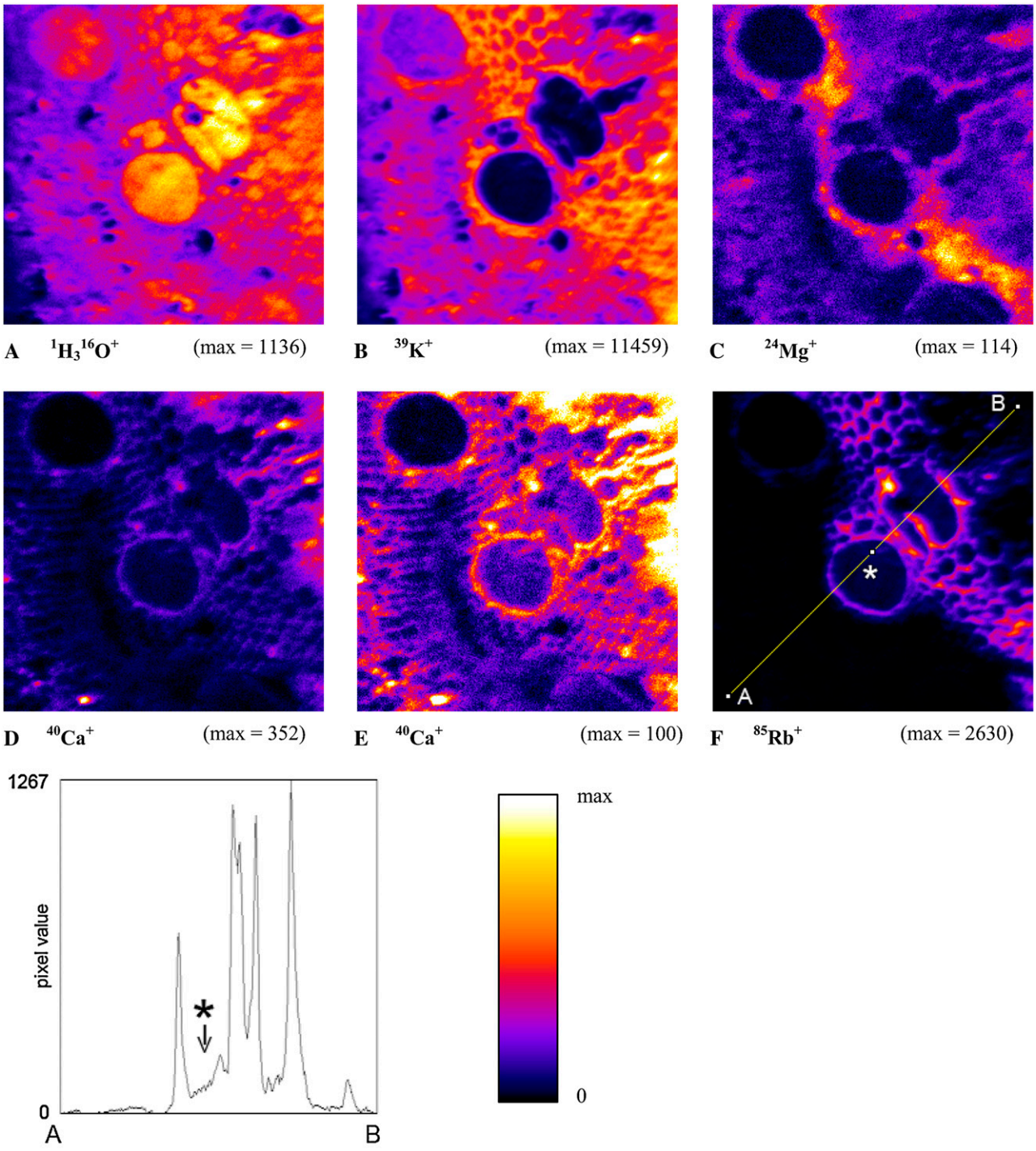

Figure 3. Cryo-ToF-SIMS images of several ion species from the surface of a frozen-hydrated sample. A slightly larger area of the same sample is shown in Figure 2A for orientation. The stem sample was taken 50 cm apical from the feeding site, 20 min after feeding Rb in a concentrated half-strength Hoagland solution to the xylem. Water (A) is represented by its highest-intensity ion, whereas K (B), Mg (C), Ca (D and E), and Rb (F) are mapped by elemental ions of the naturally most abundant isotopes. Images were acquired in the high-current bunched mode. Imaged areas are 500 × 500 μm^2 at a resolution of 256 × 256 pixels. Like all subsequent cryo-ToF-SIMS images below, each image was linearly scaled (equalized) from zero to its maximal counts per pixel, with the maximal value indicated (max =) and mapped to the indicated palette. Note that the $^{40}Ca^+$ image in E is the same image as shown in D, but equalized to a reduced max = 100 to reveal further details of lower signals. The linescan (G) was computed from the image dataset of the Rb image (F) along the path from A to B. The largest xylem vessel in the line is marked in both figures by an asterisk (*). It is the same vessel that is marked as X3 in Figure 2A.

that could be used in times of deficiency in the xylem parenchyma.

By contrast, $^{40}Ca^{+}$ images exhibited particularly high ion signals in only a few spots in the pith region in the neighborhood of the xylem vessels and in the phloem region (Fig. 3D). When the image was scaled to a fraction of the maximal signal allowing highlight clipping in these hot spots (Fig. 3E), the highest $^{40}Ca^{+}$ signals were found in the pith. Lower signals are found in the thick-walled xylem parenchyma and the phloem. Because the $^{40}Ca^{+}$ signal pattern resembles the cellular structure of the tissues, it may originate mainly from the large pools of Ca found in the cell walls (Marschner, 1995). Still lower signals originate from the cambium, the thin-walled xylem parenchyma, and the xylem vessels. Interestingly, xylem vessels X2 and X3 exhibit higher signals than vessel X1. This finding would be expected if X2 and X3 were conducting xylem vessels in which the half-strength Hoagland solution moved, whereas X1 as a nonconducting vessel remained free of the additional Ca.

Despite the fact that Na should be detectable with a relative sensitivity factor similar to that of K (Dérue, 2006b), Na could not be imaged in these samples. The results for mapping of Na^{+} were variable and signals, if any, yielded only faint and poorly structured images that could not properly be evaluated (data not shown). This must be due to low Na concentrations in the stem tissues of this natrophobic *Leguminosae* species (Marschner, 1995).

Despite the caveat regarding the unknown strength of a possible matrix effect, the specific element mappings provided indications for differences in functional specialization and degrees of maturation within different tissues. Attribution of signals to different tissue types was possible at this level of lateral resolution and image contrast. Qualitatively similar distribution patterns for $^{39}K^{+}$, $^{24}Mg^{+}$, and $^{40}Ca^{+}$ were acquired for 30 of 30 analyzed surface areas regardless of the feeding solution (data not shown). In none of the analyzed samples did we witness an indication of element redistribution due to the surface planing during sample preparation (e.g. along knife marks in cases where these were visible by cryo-SEM).

Cryo-ToF-SIMS Imaging of Rb as an Element Tracer for K at 10-μm Lateral Resolution

Studies of dynamic processes, such as the loading and unloading of xylem vessels, require the use of appropriate tracers. The suitability of Rb as an element tracer for K (e.g. in transport studies) was tested in the next step of evaluation of the cryo-ToF-SIMS imaging protocols. Figure 3F shows the cryo-ToF-SIMS image of the major isotope of Rb from the same experiment as described in Figure 3, A to E. One reason to choose Rb as an element tracer for K was the fact that it is naturally present in very low amounts in plant tissues (e.g. 2,000-fold lower compared to K in tomato [*Solanum lycopersicum*] leaves; National Institute of Standards and Technology standard reference material 1573a). Despite this low natural background, Rb could be detected in our measurements of frozen-hydrated tissue samples when no tracer was added (data not shown). Because of this combination of high detection sensitivity and low natural background, Rb tracer should be detectable in the cryo-ToF-SIMS images even in very small amounts near the background of 1/2,000 of the local K concentration. Figure 3F demonstrates that the major isotope, $^{85}Rb^{+}$, could be imaged after the 20-min feeding time in the walls of xylem vessels X2 and X3 and radial from these vessels in the surrounding thick-walled xylem parenchyma 50 cm apical of the application site. However, a clear-cut attribution of the ion signals to the apoplast and/or symplast would require a higher lateral resolution.

The wide dynamic range of the Rb signal cannot show detailed steps of signal in the limited dynamic range of the print medium. Therefore, an intensity profile derived from the dataset of this image (from bottom left A to top right corner B, plotted in Figure 3G) gives a more quantitative presentation of the Rb signals. The tracer is present in the lumen of vessel X3, as well as in the lumen of X2, but not in X1, as determined from regions of interest (data not shown). This indicates differences in xylem transport of the tracer between these vessels. In the cambium and phloem, Rb was not detectable at levels above natural background.

Cryo-ToF-SIMS Imaging of the Enriched Stable Isotope Tracer ^{41}K

Matrix effects can be ruled out when enriched stable isotopes are employed as tracers because the ratios of the isotopes are the basis for detection and quantification. Naturally occurring K is mainly composed of ^{39}K (93.2581%) and ^{41}K (6.7302%; Böhlke et al., 2005). Our own measurements obtained from entire cryo-ToF-SIMS images from three independent samples yielded a mean abundance of 93.75% ^{39}K and 6.25% ^{41}K with $3\sigma = 0.54\%$ for each of the two isotopes. With these error margins, we assume in first approximation that we can detect a ^{41}K tracer if the measured abundance exceeds our measured natural abundance by 0.54%. For the ^{41}K used in this study (enriched to 97%), this corresponds to the presence of 0.6% of the tracer in total K. On the single-pixel level or regions of interest, however, this detection sensitivity will be reduced and primarily limited by the statistical variation of the number of counts per pixel.

Cryo-ToF-SIMS Imaging at Enhanced Lateral Resolution

The distribution of the stable isotope ^{41}K supplemented as a tracer for K was investigated at increased lateral resolution to facilitate analysis at the cellular level. Higher lateral resolution was attempted in two different ways. (1) In the low-current bunched mode, the lateral resolution was improved to 6 μm at a mass

resolution of $m/\Delta m = 5{,}000$. (2) The burst-align mode offers the potential to obtain enhanced lateral resolution up to a specified value of 300 nm. However, in this measuring mode, the mass resolution is reduced to nominal mass. Therefore, it was necessary to acquire isotope images in both modes. The high mass resolution was necessary to detect the possible presence of mass interference by different ion species that might be superimposed at the mass of the selected ions and unnoticed at low mass resolution. At high mass resolution, it was possible to quantify their possible contribution to determine possible errors in images obtained at high lateral resolution.

As a point of reference for the following cryo-ToF-SIMS images within the tissue (yellow box), a cryo-SEM image is shown in Figure 4. An assembly of protoxylem and metaxylem vessels can be seen with decreasing diameters from bottom left to top right surrounded by thick-walled xylem parenchyma. Figure 4, A and B, show typical distributions of $^{39}K^+$ and $^{41}K^+$ measured in the low-current bunched mode.

Both isotope images contain a mixture of the naturally occurring isotope originating from the plant and the isotope originating from the tracer (because the tracer is not pure $^{41}K^+$, a fraction is present in the $^{39}K^+$image). Highest $^{39}K^+$ signals originate from perimeters of the xylem vessels, the thick-walled xylem parenchyma, and the pith.

The distribution of $^{41}K^+$ signals is similar, with the remarkable exception in some the protoxylem and metaxylem elements that show very high signals of $^{41}K^+$, but lower signals for $^{39}K^+$. In the case of ^{41}K, the highest signals were detected in the tangential walls of the smaller xylem vessels (Fig. 4B, center) and the xylem parenchyma, especially close to the vessels. Interestingly, the tangential parts of these vessels exhibited higher signals of $^{41}K^+$ than of $^{39}K^+$ isotope, suggesting that a substantial amount of K detected in these structures originated from the ^{41}K tracer. The image of the ^{41}K isotope fraction is calculated from Figure 4, B and C, and is displayed in Figure 4D. The maximal value per pixel of total $^{41}K^+$ was 47%. This corresponds to a maximal fraction of the tracer of 45% if the small amount of ^{39}K in the tracer solution is also corrected for (see ''Materials and Methods''). Figure 4D shows that the largest fraction of ^{41}K is found in the xylem lumina. Additional signals originate from the xylem parenchyma left and top left of the central vessel. These distribution patterns were typical of all four images from three plants fed with solution 2. In control samples where no ^{41}K had been applied, the ratio of $^{41}K^+$ to ($^{39}K^+ + {}^{41}K^+$) was homogeneous and no relevant contrast was visible (data not shown).

We checked for possible mass interferences for the K isotopes in the spectra taken at nominal mass resolution by inspecting high mass resolution spectra from entire images being recorded in the low-current bunched mode in samples where ^{41}K tracer was not used. The signal at nominal mass resolution was 98.75% identified as ^{39}K and 1.25% in one interfering peak, most likely C_3H_3. There were three peaks at the position of ^{41}K at nominal mass resolution. ^{41}K contributed about 83% and the interfering peaks (presumably carbohydrates) contributed about 17%. This demonstrated that ^{39}K can be imaged at high lateral resolution in our samples at the nominal mass resolution of the burst-align mode, with only minor mass interferences. Images of ^{41}K must be interpreted with some caution and may require verification of ^{41}K distribution patterns by complementary high mass resolution imaging in the low-current bunched mode.

Imaging at 1-μm Lateral Resolution with Nominal Mass Resolution

Images of the same sample area acquired with the burst-align mode are displayed in Figure 5. Limiting the measuring time to a 4-h time period per image set required a restriction in image area, in this example to $195 \times 195\ \mu m^2$. This still supplied a view covering the protoxylem and metaxylem with surrounding tissues. The lateral resolution was slightly better than 1 μm as suggested by line scans across cell walls of frozen-hydrated tissue samples (data not shown). This improved resolution can give a more detailed view of the element distributions not yet visible in Figure 4. For example, the very small xylem parenchyma cells abutting the xylem vessels, which could not be identified as individual cells in Figure 4, can be identified in the images of $^1H_3{}^{16}O^+$ (Fig. 5A). Interestingly, subcellular dendritic ice crystal structures could be imaged in this measuring mode as demonstrated in Figure 5A.

The improved resolution refines the results already seen in the images in Figures 3 and 4, as exemplified by the K images. High $^{39}K^+$ signals (Fig. 5C) are found especially in very small parenchyma cells directly adjacent to the xylem vessels. The high signal apparently originates from the cell borders, although the contributions from the cytoplasm and/or the cell walls cannot be allocated precisely. Interestingly the tangential walls of the xylem vessels display rather low $^{39}K^+$ signals (Fig. 5C). By contrast, these structures were particularly prominent in the $^{41}K^+$ image (Fig. 5D), confirming the findings of Figure 4C. The corresponding map of $^{41}K/(^{39}K + {}^{41}K)$ (Fig. 5E) shows the maximal fraction of total ^{41}K as 53%, corresponding to a maximal fraction of the tracer of 51%. It is more clearly visible in Figure 5E than in Figure 4D that the tracer of K transport was located predominantly in the xylem vessels, but that it had also spread into the neighboring tissue. Seemingly equal fractions of ^{41}K were present in the vessel lumina and walls. Lower, but visible, ^{41}K percentages delineate the cell borders of the xylem parenchyma.

Imaging of Supplemented Na

Interestingly, there is no mass interference at $^{23}Na^+$. Because Na is extremely difficult to map using microbeam techniques unless present in high concentra-

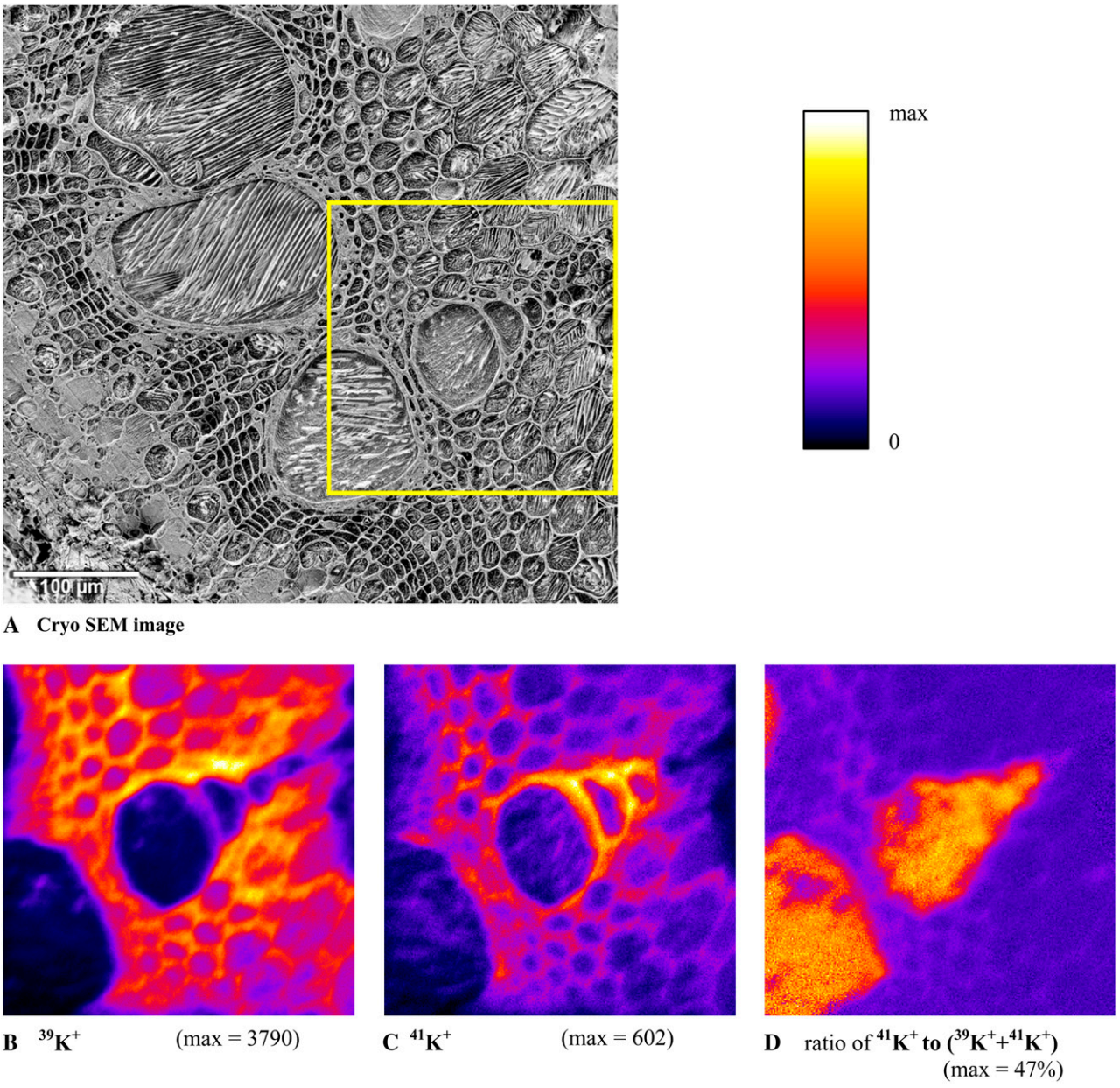

Figure 4. A to D, Cryo-SEM image (A) and cryo-ToF-SIMS images (B–D) of the surface of a bean stem cross section. The SEM image (A) was obtained after analysis with cryo-ToF-SIMS and freeze etching. The tissue details described in Figure 2A can be seen here as well. The stem sample was taken 50 cm apical from the feeding site 20 min after feeding enriched ^{41}K as a tracer to the xylem. The isotope maps show the two major isotopes $^{39}K^+$ (B) and $^{41}K^+$ (C). The analyzed area is indicated by the yellow box in A and was selected to cover the protoxylem and metaxylem. The images were acquired in the low-current bunched mode. The imaged area is $229 \times 229\ \mu m^2$ with 256×256 pixels. The calculated map of the ratio $^{41}K^+$ to ($^{39}K^+ + {}^{41}K^+$) that indicates the distribution of the ^{41}K tracer expressed in percent is shown in D.

tions, it was straightforward to test whether imaging of $^{23}Na^+$ was possible at high lateral resolution. Whereas we were again unable to image Na in control plants, we tested whether supplemented Na could be detected. Sodium was supplemented to the transpiration stream as 2.5 mM NaCl in the stable isotope tracer solution (solution 2). Figure 5B shows a highly detailed distribution of $^{23}Na^+$ with high signals in the xylem parenchyma. This finding is compatible with the previously published assumption that Na accessing in the transpiration stream of natrophobic species, especially in *Phaseolus*, is relocated into xylem parenchyma (Jacoby, 1965; Rains, 1969; DeBoer and Volkov, 2003).

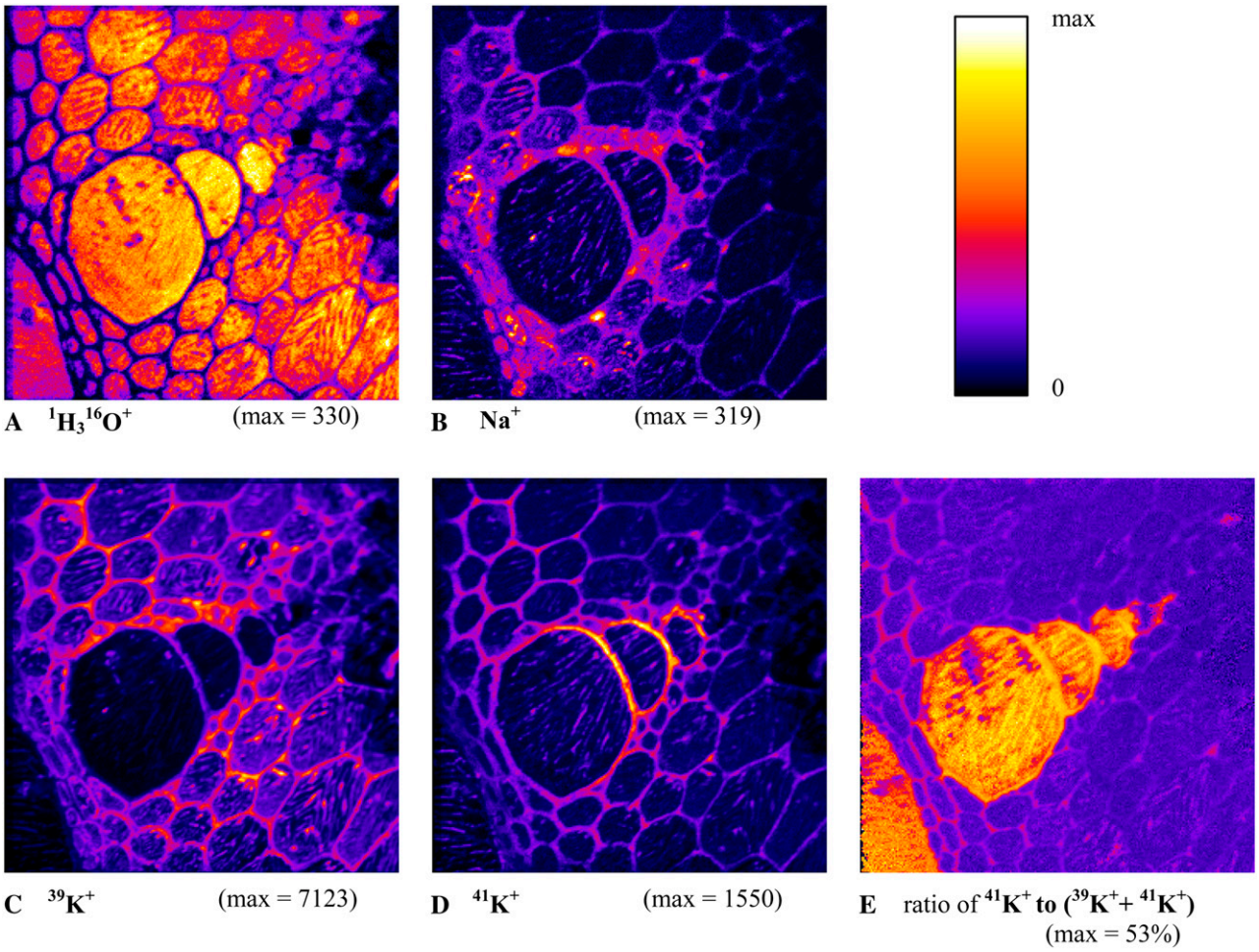

Figure 5. Cryo-ToF-SIMS mappings of the sample shown in Figure 4, but at higher magnification and enhanced lateral resolution obtained in the burst-align mode. A to D, Maps of $^{1}H_3{}^{16}O^+$, $^{23}Na^+$, $^{39}K^+$, and $^{41}K^+$, respectively. E, Calculated map of the ratio $^{41}K^+$ to ($^{39}K^+$ + $^{41}K^+$) expressed in percent. Note that in the selected measuring mode mass interferences on mass 41 could contribute up to 17% to the $^{41}K^+$ ion signal. The area was imaged with 256 × 256 pixels covering 195 × 195 μm^2.

Assigning Ion Distributions to Detailed Anatomical Structures

The cryo-ToF-SIMS images obtained at the high lateral resolution contain such a high level of detail that analysis of subcellular structures appeared possible. However, because each image relates to only one single ion in the tissue, the unambiguous identification of structures within the ion images still proved difficult. We therefore superimposed ion images onto cryo-SEM images of the same areas after freeze etching. Two such overlays are shown in Figure 6. Two different magnifications originating from the same cryo-ToF-SIMS and cryo-SEM datasets are shown to allow orientation within the tissue, as well as an optimal view of cellular and subcellular details. Figure 6A shows an overlay of the K isotope ratio image already shown in Figure 5E over the corresponding cryo-SEM. It is already possible to marginally distinguish between symplastic and apoplastic areas. This confirms the finding from Figure 5E that large fractions of $^{41}K^+$ were found in the cell borders of thick-walled xylem parenchyma, but now these signals can be clearly attributed to the cell walls of this tissue.

Zooming in to a higher magnification (Figure 6B) reveals subcellular structures in more detail (e.g. cytoplasm and cell walls). In this case, the overlaying cryo-ToF-SIMS image shows the $^{39}K^+$ isotope (from Fig. 5C) that represents predominantly the K in the plant before onset of the labeling. $^{39}K^+$ is not primarily detected in the apoplast, but high signals originate from the cytoplasm, especially pronounced in the cytoplasm-rich parenchyma cells abutting the xylem vessels. Subcellular differences (e.g. differentiation between cytoplasm, vacuole, and organelles) can be observed in these cells. Several larger parenchyma and pith cells show extended vacuoles and narrow rims of cytoplasm together with plasma pockets around the organelles. Figure 6B reveals that $^{39}K^+$ signals found in the vacuoles are lower than in the cytoplasm. This is consistent with reported findings (Leigh, 2001) with a

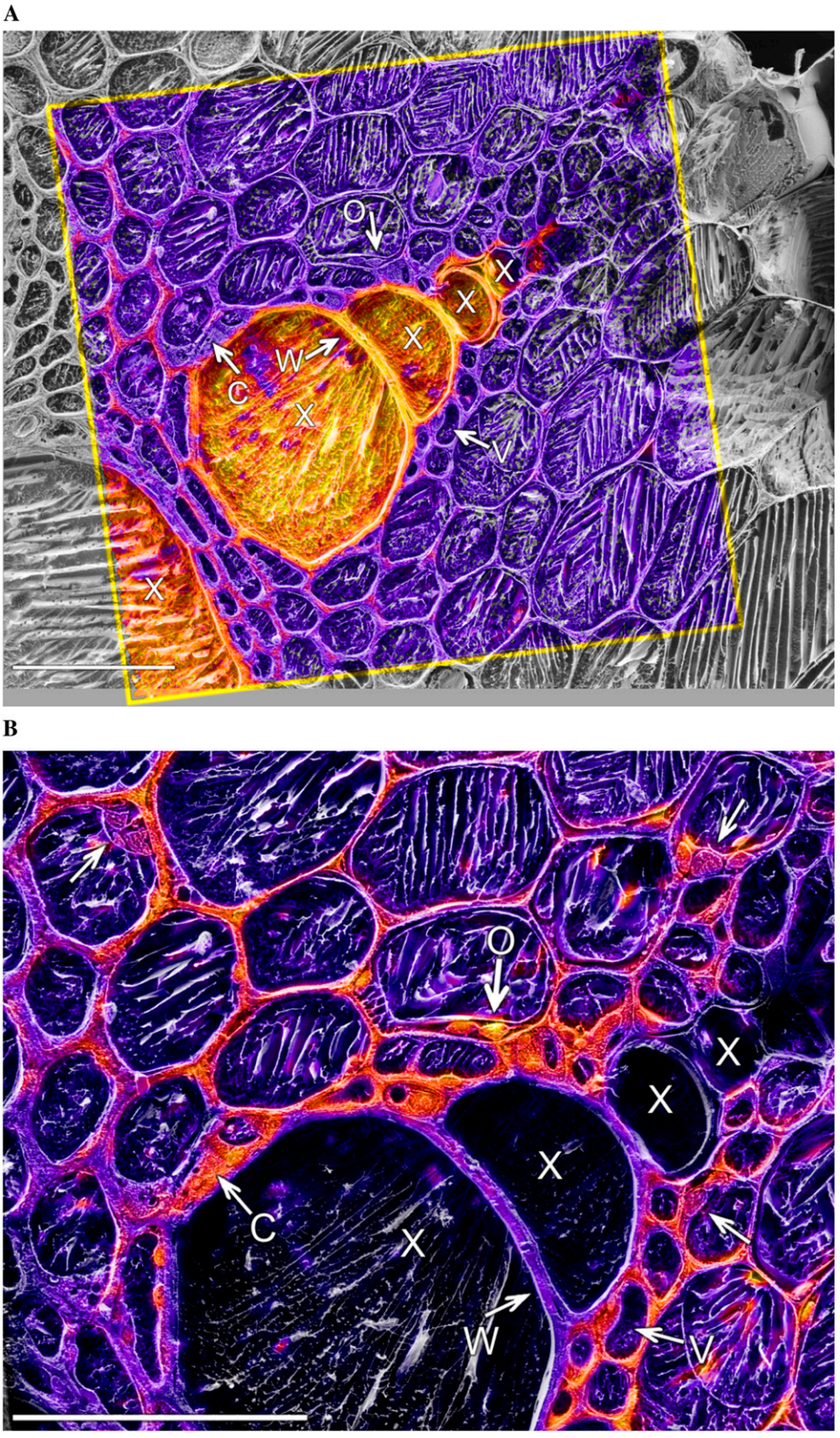

Figure 6. Cryo-ToF-SIMS, superimposed onto corresponding cryo-SEM images of the same area, presented as overlays. The cryo-SEM image was obtained after cryo-ToF-SIMS analysis and subsequent freeze etching. Figure 6A shows the ratio $^{41}K^+$ to ($^{39}K^+ + {}^{41}K^+$). It covers the entire area analyzed by cryo-ToF-SIMS plus a small margin for better orientation within the tissue. The ratio image was already shown separately in Figure 5E. Figure 6B images the isotope $^{39}K^+$ that was also shown above as separate image in Figure 5C. The view was zoomed in for this figure to better visualize the structural details at the print size. Among the subcellular structures visible are the xylem vessels (X), cell walls (W), vacuoles (V), and cytoplasm (C) with contained organelles (O). For clarity of the underlying structures, background subtraction and transparency adjustment were applied. The unlabeled arrows indicate thin rims of cytoplasm with plasma pockets. The micron markers in both images represent 50 μm.

different experimental approach (triple-barreled ion-sensitive microelectrodes), showing high levels of K (80–100 mM) in the cytoplasm and up to 100 mM in the vacuoles.

CONCLUSION AND FUTURE PERSPECTIVE

Three cryogenic techniques, namely (1) specimen preparation of shock-frozen tissue samples, (2) cryo-ToF-SIMS, and (3) cryo-SEM were improved and combined for the task of nutrient element imaging and tracer analysis in tissues for the study of transport processes in plants.

1. Specimen preparation by cryo-fracturing and planing surfaces produced samples adequate for cryo-ToF-SIMS analysis. This avoids the necessity to produce cryo-sections, which is considered difficult, if not impossible, for many tissues.
2. High-quality images were obtained by cryo-SEM, allowing tissue identification and recognition of subcellular structures. Thus, despite the large sample sizes of approximately 2 mm, sufficient structural preservation could be obtained by shock freezing and maintained throughout the cryogenic workflow, including shuttle transfers from sample preparation through cryo-ToF-SIMS to cryo-SEM.
3. Lateral resolution of cryo-ToF-SIMS at high mass resolution ranged in large area nutrient surveys from 10 to 6 μm. The high mass resolution was required for the unambiguous identification of the major isotopes of nutrient cations and their separation from possibly interfering ions.
4. High lateral resolution cryo-ToF-SIMS at reduced mass resolution allowed ion imaging at tissue details, such as assemblies of xylem vessels and surrounding xylem parenchyma with subcellular details at 1-μm resolution. Possible uncertainties of mass interferences were quantified from images at high mass resolution of the same areas.
5. The combination of high lateral resolution cryo-ToF-SIMS with cryo-SEM images in overlay images allowed the mapping of selected ions to cellular and subcellular structures, including a distinction between apoplastic and symplastic localization.
6. The elemental tracer Rb was applied to the transpiration stream and could be detected with high sensitivity by cryo-ToF-SIMS apical of the application site. Na supplemented at 2.5 mM could be detected, yielding images of high detail. However, quantification is not advisable due to a possible matrix effect.
7. The isotopic tracer ^{41}K could be imaged at a lower sensitivity of detection than Rb, but ratio images of ^{41}K can be used to quantify the percentage of total K, thus providing a powerful tool to track K movement.

The study revealed that cryo-ToF-SIMS is well suited to monitor distributions of nutrients in plant tissue samples and to detect tracers down to the subcellular level. Both types of tracer could be imaged after transport within the xylem and radially translocated into the surrounding tissue. Enriched (stable) isotope tracers can be imaged with cryo-ToF-SIMS to trace nutrients unaffected by matrix effects and topography effects, thus allowing quantification of the tracer fraction. Physiological effects of tracer addition can be completely eliminated when the tracer is applied at unchanged concentration by changing isotopic composition only. Besides ^{41}K used in this pilot study, suitable enriched stable isotopes are available for most elements. For several nutrients, such as Mg and Ca, more than one isotope is available to allow for simultaneous multi-element multitracer analysis. To our knowledge, no other technique can detect several tracers simultaneously at a similar lateral resolution and sensitivity.

Possible future applications in plant nutrition studies could focus on loading and unloading sites of the long-distance transport systems or on the penetration of diverse tissues by different nutrients from conducting tissue. Another field of application is in plant phenotyping, especially ecotypes and mutants obtained by genetic engineering. Studies on the movement of mineral nutrients (e.g. across the endodermis) or on the accessibility of different tissues for specific elements traveling in the xylem can be helpful in characterization particularly of mutants modified in ion transport.

MATERIALS AND METHODS

Plant Material

French bean (*Phaseolus vulgaris* 'Shiny Fardenlosa') plants were grown from seeds in 1.7-L pots with standard soil substrate (type ED 73; Einheitserde) in a growth chamber with a 12-h light/12-h dark cycle, a temperature of 20°C to 25°C, and a relative humidity of 35% to 45%. Illumination with photosynthetically active radiation (PAR) of 300 μmol m^{-2} s^{-1} was obtained with commercial fluorescent lamps (15 × 36-W; Fluora). Alternatively, plants were grown throughout the year under controlled greenhouse conditions with a day/night regime of 26°C/18°C and 45%/80% relative humidity. During the 16-h photoperiod, irradiance was enhanced by movable high-pressure sodium lamps, if required, to ensure that the natural light intensity never fell below a PAR value of about 390 μmol m^{-2} s^{-1}. Automatic watering of all plants occurred twice a day. Plants were used for experiments at an age of approximately 4 weeks when at least three mature trifoliate leaves had developed.

Tracer Application

Two different tracer solutions containing either the elemental tracer Rb or the isotope tracer ^{41}K were used. The Rb tracer (solution 1) consisted of 10 mM RbCl and 5 mM CsCl in half-strength Hoagland solution (modified after Hoagland and Arnon, 1950) containing 2.5 mM KNO_3, 2.5 mM $Ca(NO_3)_2$, 1 mM $MgSO_4$, and 0.5 mM KH_2PO_4 at pH 5.1 and trace elements as 5 μM $MnCl_2$, 0.5 μM $CuSO_4$, 0.5 μM $ZnSO_4$, 25 μM H_3BO_3, and 0.25 μM $NaMoO_4$. The enriched-stable isotope tracer solution (solution 2) was a multielement tracer solution consisting of $^{26}MgCl_2$ (enriched to 96% ^{26}Mg; natural abundance 10.0%), ^{41}KCl (enriched to 97% ^{41}K; natural abundance 6.7%), $^{44}CaCl_2$ (enriched to 96% ^{44}Ca; natural abundance 2.1%), and $Na^{15}NO_3$ (enriched to 94% ^{15}N; natural abundance 0.4%), each at 2.5 mM concentration in deionized water. $Na^{15}NO_3$ was obtained from Sigma-Aldrich, whereas all other stable isotopes were purchased from Medgenix.

In separate experiments, either of the tracer solutions was fed into the transpiration stream by cutting the shoot of a bean plant under water a few

centimeters above the root and rapidly transferring the wet cut end into the tracer solution. The Rb tracer solution was applied in the laboratory at a PAR of 100 μmol m^{-2} s^{-1} (400-W HQI lamp; Osram), a temperature of 24°C, and a relative humidity of 45%, whereas the stable isotope and combined tracer solutions were fed in the growth chamber. During a subsequent feeding period of 20 min, the shoot usually took up about 2 to 3 mL of the Rb tracer solution and 4 mL of the stable isotope tracer solution, respectively. We found similar uptake as measured by weight losses due to transpiration using comparable control plants placed next to the experimental plants.

Preparation of Frozen-Hydrated Tissue Samples

As termination of the feeding procedure, stem samples of approximately 4-cm length were quickly excised with a scalpel blade from the first and second internode above the primary leaves and mounted in tightly fitting copper rivets by the aid of 0.6 M Suc solution (Sigma-Aldrich). These sample-rivet assemblies were rapidly shock frozen by plunging them into melting propane (−189°C). The time period from excision to freezing was less than 30 s.

During the subsequent procedures of sample preparation and measurement, the ambient temperature was continuously controlled, not exceeding −130°C. Frozen samples were trimmed at liquid nitrogen temperature to protrude <3 mm from the rivets and stored under liquid nitrogen. Clean and even surfaces, as needed for cryo-ToF-SIMS analysis, were obtained by planing the samples with the aid of a microtome. To this end, a sample-rivet assembly was mounted under liquid nitrogen on a modified commercial sample holder (BU 012092-T; BAL-TEC) that had been mechanically adapted to receive the rivet. The sample holder was transferred from the liquid nitrogen storage container to the freeze-fracturing unit (MED 020/GBE; BAL-TEC) by use of a so-called cryo-shuttle (VCT-100; BAL-TEC). The shuttle was filled with dry cryogenic nitrogen gas and the sample holder introduced through a dry cryogenic nitrogen atmosphere. The shuttle was closed and the sample moved to the freeze-fracturing unit. After connection to the MED 020, the shuttle was evacuated and the sample holder transferred to the precooled sample stage of the MED 020. At a temperature of approximately −150°C and a pressure of 10^{-3} Pa, the sample was planed with a hard metal knife of a built-in microtome under stereomicroscopic control by first removing a few 10-μm slices from the top of the sample and then removing 5-μm-thick slices until the surface was reasonably flat. After planing, the sample was again introduced into the cryo-shuttle while maintaining high vacuum and protecting the specimen from heating and surface contamination by a liquid nitrogen-cooled cryo-shield. The sample was subsequently transferred to the cryo-SEM and/or the cryo-ToF-SIMS via the shuttle across the respective airlock systems. Upon arrival on the cryo-stages of both instruments typically after approximately 15-min transfer time, the temperature of the sample holder never exceeded −130°C. The shuttle vacuum was always below 1×10^{-3} Pa after transfer.

Cryo-SEM

A LEO Gemini VP 1550 SEM (Zeiss) with a cold-field emission electron source was used for imaging of the surfaces of frozen-hydrated samples. The instrument is equipped with a BAL-TEC cryo-stage (BAL-TEC) and an airlock for the cryo-shuttle. The samples were imaged at an acceleration voltage of 1.8 keV at a stage temperature below −120°C and a pressure of 2×10^{-3} Pa.

If freeze etching was required, the temperature of the sample stage was transiently raised to −90°C. The etching process was monitored by continuous scanning of the sample and stopped as required for imaging of the tissue structure by interrupting the stage heating, typically after 2 to 5 min. Overlays of ion images superimposed over SEM images were produced using Adobe Photoshop CS3 and overlay mode for image blending. SEM images were optimized for printing using limits and curves settings in Photoshop.

Cryo-ToF-SIMS

For the element and isotope imaging performed in this study, a ToF-SIMS IV mass spectrometer (IONTOF) was used. A separate airlock system allowed the transfer of a sample between the shuttle and the cryo-stage. The cryo-stage was based on the IONTOF heat/cool sample holder that had been modified to reach and maintain temperatures down to −150°C. For all reported measurements, the sample temperature was kept below −130°C.

To remove a possibly deposited thin layer of ice or other possible surface contamination, an area of 750 × 750 μm^2 was presputtered with an O_2^+ ion beam at 2 keV and 400 nA for 90 s, resulting in an ion dose density of 4×10^{16} ions cm^{-2}. In a silicon sample, assuming a sputter yield of one sputtered particle from each primary ion, this would presumably remove 10 nm from the surface of the sample.

For cryo-ToF-SIMS analysis a pulsed mass-filtered 25 keV Bi^+ ion beam was used. The ion beam current was between 0.2 and 1.2 pA and resulted in a primary ion dose density between 1.3×10^{13} and 6.9×10^{13} ions cm^{-2}. In a silicon sample, this would result in the removal of less than 1 nm from the surface of the sample during analysis. The sputtered secondary ions were extracted with 2 kV into a reflectron ToF mass analyzer. Only positively charged ions were analyzed. A complete secondary ion spectrum was recorded for each pulse and each pixel. To prevent charging of the sample surface, a low-electron energy flood gun was used.

Three different modes of operation were used with differently weighted compromises for the counteractive parameters of mass resolution, lateral resolution, and time of measurement required for a sufficient signal:

1. The high-current bunched mode was used for large area views (500 × 500 μm^2; see Fig. 3). To achieve high mass resolution in this mode, the primary ion pulses (5 to 15 ns) were compressed by a bunching device to produce shorter pulses of 1 to 2 ns. This resulted in a mass resolution $m/\Delta m$ of 3,500 (at mass 41). As a trade-off, the energy spread introduced by the buncher and the resulting chromatic aberration limited the lateral resolution to 10 μm as determined by knife edge scans. This mode employs the highest primary ion density (875 ions/pulse) of all modes and therefore offers the highest ion yield per primary ion pulse.
2. The low-current bunched mode was preferred for imaging with high lateral and high mass resolution (see Fig. 4). It is identical to the high-current bunched mode described above, but with a reduced primary ion density (190 ions/pulse). Therefore, the lowered ion yield per pulse allowed only for smaller raster sizes without extensive prolongation of the measurement time, thereby improving the mass resolution $m/\Delta m$ to 5,000 (at mass 41). The advantage is the improved lateral resolution of 6 μm (determined by knife edge scans).
3. The burst-align mode was used for detailed mapping (see Fig. 5). Pulses were not bunched, which allowed for an improved lateral resolution of approximately 1 μm (knife edge scans), but limited the mass resolution to nominal mass. The low primary ion density (120 ions/pulse), resulting in low ion yield per pulse, allowed only small raster sizes without extensive prolongation of the measurement time.

A Poisson correction algorithm (Stephan et al., 1994) as part of the ion-image software (IONTOF) was used in all modes for compensation of dead-time effects of the detector at high count rates. Based on the number of measurement cycles and the number of detected counts, the probability of a missed count event was calculated and added to the counted number. The resulting number of counts per pixel within the indicated mass window integrated over all measurement is referred to as signal in the text.

To compute the true percentage of the ^{41}K isotope tracer (C_{tracer}) based on the measured ^{39}K and ^{41}K images, we used the following formula:

$$C_{\text{tracer}} = (41_{\text{measured fraction}} - 41_{\text{natural fraction}})/(41_{\text{fraction of the tracer}} - 41_{\text{fraction of natural isotope}}).$$

This corrects for the ^{41}K fraction present in the total K in the plant and the ^{39}K fraction in the enriched tracer.

ACKNOWLEDGMENTS

We are very grateful to Alexandra Ley for performing light microscopy on bean stem cross sections as a valuable aid for orientation in the cryo-ToF-SIMS instrument. We thank Hans-Peter Bochem and the Institute of Bio- and Nanosystems 2 for the liberal use of their SEM facilities. Special support came from Marion Roeb and Beate Uhlig for plant cultivation. Andreas Averesch and the ICG workshop, especially Elmar Mommertz, contributed general technical assistance. Michael Thorpe, Hinrich Lühring, and Vicky Temperton helped with critical reading of the manuscript.

Received September 14, 2007; accepted May 26, 2008; published June 20, 2008.

LITERATURE CITED

Böhlke JK, de Laeter JR, De Bièvre P, Hidaka H, Peiser HS, Rosman KJ, Taylor PD (2005) Isotopic composition of the elements, 2001. J Phys Chem Ref Data **34:** 57–67

Canny MJ (1993) The transpiration stream in the leaf apoplast: water and solutes. Philos Trans R Soc Lond B Biol Sci **341:** 87–100

Cliff B, Lockyer NP, Corlett C, Vickerman JC (2003) Development of instrumentation for routine ToF-SIMS imaging analysis of biological material. Appl Surf Sci **203-204:** 730–733

Colliver TL, Brummel CL, Pacholski ML, Swanek FD, Ewing AG, Winograd N (1997) Atomic and molecular imaging at the single-cell level with ToF-SIMS. Anal Chem **69:** 2225–2231

DeBoer AH, Volkov V (2003) Logistics of water and salt transport through the plant: structure and functioning of the xylem. Plant Cell Environ **26:** 87–101

Dérue C, Gibouin D, Demarty M, Verdus MC, Lefebvre F, Thellier M, Ripoll C (2006a) Dynamic-SIMS imaging and quantification of inorganic ions in frozen-hydrated plant samples. Microsc Res Tech **69:** 53–63

Dérue C, Gibouin D, Lefebvre F, Rasser R, Robin A, Le Sceller L, Verdus MC, Demarty M, Thellier M, Ripoll C (1999) A new cold stage for SIMS analysis and imaging of frozen-hydrated biological samples. J Trace Microprobe Tech **17:** 451–460

Dérue C, Gibouin D, Lefebvre F, Studer D, Thellier M, Ripoll C (2006b) Relative sensitivity factors of inorganic cations in frozen-hydrated standards in secondary ion MS analysis. Anal Chem **78:** 2473–2477

Dickinson M, Heard PJ, Barker JH, Lewis AC, Mallard D, Allen GC (2006) Dynamic SIMS analysis of cryo-prepared biological and geological specimens. Appl Surf Sci **252:** 6793–6796

Enns LC, McCully ME, Canny MJ (1998) Solute concentrations in xylem sap along vessels of maize primary roots at high root pressure. J Exp Bot **49:** 1539–1544

Fricke W, Leigh RA, Tomos AD (1996) The intercellular distribution of vacuolar solutes in the epidermis and mesophyll of barley leaves changes in response to NaCl. J Exp Bot **47:** 1413–1426

Goldsmith JG, Lazof DB, Schroeder WH, Kuhn AJ, Rufty TW, Linton RW (1993) Application of secondary ion image analysis for quantification of isotope and elemental nutrient tracers in plant tissues. *In* A Benninghoven, Y Nihei, R Shimizu, HW Werner, eds, Secondary Ion Mass Spectromtry SIMS IX. John Wiley & Sons, Chichester, UK, pp 824–827

Goldstein JI, Romig AD, Newbury DE, Lyman CE, Echlin P, Fiori C, Joy DC, Lifshin E (1992) Scanning Electron Microscopy and X-Ray Microanalysis, Ed 2. Plenum Press, New York

Halperin SJ, Lynch JP (2003) Effects of salinity on cytosolic Na^+ and K^+ in root hairs of *Arabidopsis thaliana*: *in vivo* measurements using the fluorescent dyes SBFI and PBFI. J Exp Bot **54:** 2035–2043

Hedrich R, Schroeder JI (1989) The physiology of ion channels and electrogenic pumps in higher plants. Annu Rev Plant Physiol **40:** 539–569

Herdel K, Schmidt P, Feil R, Mohr A, Schurr U (2001) Dynamics of concentrations and nutrient fluxes in the xylem of *Ricinus communis*—diurnal course, impact of nutrient availability and nutrient uptake. Plant Cell Environ **24:** 41–52

Hoagland DR, Arnon DI (1950) The water-culture method for growing plants without soil. Calif Agr Exp Sta Cir **347:** 1–39

Jacoby B (1965) Sodium retention in excised bean stems. Physiol Plant **18:** 730–739

Jeschke WD (1970) Über die Verwendung von ^{86}Rb als Indikator für Kalium, Untersuchungen am lichtgeförderten ^{42}K/K- und ^{86}Rb/Rb-Influx bei *Elodea densa*. Z Naturforsch **25:** 624–630

Küpper H, Zhao FJ, McGrath SP (1999) Cellular compartmentation of zinc in leaves of the hyperaccumulator *Thlapsi caerulescens*. Plant Physiol **119:** 305–311

Lazof D, Linton RW, Volk RJ, Rufty TW (1992) The application of SIMS to nutrient tracer studies in plant physiology. Biol Cell **74:** 127–134

Leigh RA (2001) Potassium homeostasis and membrane transport. J Plant Nutr Soil Sci **164:** 193–198

Lohaus G, Hussmann M, Pennewiss K, Schneider H, Zhu JJ, Sattelmacher B (2000) Solute balance of a maize (*Zea mays* L.) source leaf as affected by salt treatment with special emphasis on phloem re-translocation and ion leaching. J Exp Bot **51:** 1721–1732

Marschner H (1995) Mineral Nutrition of Higher Plants, Ed 2. Academic Press, London

Marschner H, Schimansky C (1968) Unterschiedliche Aufnahme von Kalium und Rubidium durch Gerste. Naturwissenschaften **55:** 499

Mühling KH, Läuchli A (2000) Light-induced pH and K^+ changes in the apoplast of intact leaves. Planta **212:** 9–15

Rains DW (1969) Cation absorption by slices of stem tissue of bean and cotton. Experientia **25:** 215–216

Rangarajan S, Tyler BJ (2006) Topography in secondary ion mass spectrometry images. J Vac Sci Technol A **24:** 1730–1736

Reintanz B, Szyroki A, Ivashikina N, Ache P, Godde M, Becker D, Palme K, Hedrich R (2002) AtKC1, a silent *Arabidopsis* potassium channel alpha-subunit modulates root hair K^+ influx. Proc Natl Acad Sci USA **99:** 4079–4084

Rowan A, McCully ME, Canny MJ (2000) The origin of the exudate from cut maize roots. Plant Physiol Biochem **38:** 957–967

Rygol J, Pritchard J, Zhu JJ, Tomos D, Zimmermann U (1993) Transpiration induced radial turgor pressure gradients in wheat and maize roots. Plant Physiol **103:** 493–500

Schroeder WH, Fain GL (1984) Light-dependent calcium release from photoreceptors measured by laser micro-mass analysis. Nature **309:** 268–270

Schroeder WH, Frings D, Stieve H (1980) Measuring calcium uptake and release by invertebrate Astacus leptodactylus photoreceptor cells by laser microprobe mass spectroscopy. Scan Electron Microsc **606:** 647–654

Shaul O, Hilgemann DW, de-Almeida-Engler J, Van Montagu M, Inzé D, Galili G (1999) Cloning and characterization of a novel Mg^{2+}/H^+ exchanger. EMBO J **18:** 3973–3980

Stephan T, Zehnpfennig J, Benninghoven A (1994) Correction of dead time effects in time-of-flight mass spectrometry. J Vac Sci Technol A **12:** 405–410

Storey R, Leigh RA (2004) Processes modulating calcium distribution in citrus leaves. An investigation using x-ray microanalysis with strontium as a tracer. Plant Physiol **136:** 3838–3848

Tomos AD, Leigh RA (1999) The pressure probe: a versatile tool in plant physiology. Annu Rev Plant Physiol **50:** 447–472

Vickerman JC (2001) ToF-SIMS—an overview. *In* J Vickerman, D Briggs, eds, TOF-SIMS: Surface Analysis by Mass Spectrometry. IM Publishing, Charlton and Surface Spectra Limited, Manchester, UK, pp 1–40

Wegner LH, Zimmermann U (2002) On-line measurements of K^+ activity in the tensile water of the xylem conduit of higher plants. Plant J **32:** 409–417

Williams ML, Thomas BJ, Farrar JF, Pollock CJ (1993) Visualizing the distribution of elements within barley leaves by energy dispersive X-ray image maps (EDX maps). New Phytol **125:** 367–372

Wilson RG, Stevie FA, Magee CW (1989) Secondary Ion Mass Spectroscopy. John Wiley & Sons, New York